Effects of eddies on an ocean observing system with profiling floats: Idealized simulations of the Argo array

Igor Kamenkovich,[1] Wei Cheng,[2] Claudia Schmid,[3] and D. E. Harrison[2]

Received 22 December 2010; revised 18 February 2011; accepted 11 March 2011; published 8 June 2011.

[1] This study aims at evaluating effects of the mesoscale variability on the expected accuracy of reconstruction of temperature, salinity, and velocities from the Argo measurements and trajectories. For this purpose, an idealized observing system with profiling floats is simulated in a high-resolution ocean model of the North Atlantic set up to produce annual mean hydrography and circulation. The simulations with and without mesoscale variability are compared, and the effects of the time mean and mesoscale eddy–induced advection are effectively separated and investigated. The results demonstrate several effects of mesoscale eddies on the expected accuracy of the Argo-based reconstructions of temperature, salinity, and horizontal velocities. In most of the domain, the eddies help to achieve uniform spatial coverage. The effects of eddy advection on reconstruction errors are, however, complex but moderate in most of the domain. High-frequency variability in temperature and salinity leads to enhancement of reconstruction errors, especially if the sampling is carried out for only a few years. The reconstruction of horizontal velocities from trajectories of the profiling floats is capable of detecting multiple zonal jets which have been observed already. The reconstruction of the meridional velocities is significantly less reliable, primarily due to a small signal-to-noise ratio in the in the interior of domain.

Citation: Kamenkovich, I., W. Cheng, C. Schmid, and D. E. Harrison (2011), Effects of eddies on an ocean observing system with profiling floats: Idealized simulations of the Argo array, *J. Geophys. Res.*, *116*, C06003, doi:10.1029/2010JC006910.

1. Introduction

[2] The Argo array has been brought up to the full strength and is now providing the oceanographic community with reliable three-dimensional global measurements of the ocean temperature and salinity. The oceanic variables reconstructed from these unique data are now being widely used in many studies that describe the current oceanic conditions and aim at detecting and analyzing changes of these conditions. The importance of these studies calls for an assessment of the accuracy of the reconstructions of the ocean state based on the Argo data. In this regard, observation system simulation experiments, or OSSEs [*Arnold and Dey*, 1986], can provide valuable information on the expected accuracy of such reconstructions. The technique has been used for the analysis of different ocean observing systems in ocean models of varying complexity [e.g., *Kindle*, 1986; *Barth and Wunsch*, 1990; *Bennett*, 1990; *Hernandez et al.*, 1995; *Hackert et al.*, 1998; *Schiller et al.*, 2004; *Ballabrera-Poy et al.*, 2007; *Vecchi and Harrison*, 2007; *Griffa et al.*, 2006]. In an OSSE, the actual model-simulated values of temperature and salinity are known precisely and can be readily compared to the reconstructed fields from the subsampled data set. The difference, the "reconstruction errors," can be calculated and analyzed, together with the factors that affect the size and spatial distribution of the errors.

[3] *Kamenkovich et al.* [2009a] utilized a global coarse-resolution model and demonstrated that reconstruction errors can be large in regions with strong advection, such as the Gulf Stream and the Antarctic Circumpolar Current. The errors were particularly significant in the magnitude of year-to-year variability. The adverse effect of the mean oceanic advection on the expected accuracy of the Argo-based reconstructions was further demonstrated by the overall reduction in the reconstruction errors in the simulation in which the Argo floats were not allowed to move. The importance of advection in *Kamenkovich et al.*'s [2009a] study, however, was most likely underestimated given the coarse resolution of the model, and the resulting weakness of the currents.

[4] Movements of floats by intense oceanic currents affect the accuracy of reconstruction in a number of ways. Strong mean currents, such as the Gulf Stream and North Atlantic Current, will significantly displace Argo floats during the 10 day sampling interval. As demonstrated by *Kamenkovich et al.* [2009a], this displacement can complicate reconstruction of the time-dependent oceanic state and even lead

[1]Rosenstiel School of Marine and Atmospheric Science, University of Miami, Miami, Florida, USA.
[2]Joint Institute for the Study of the Atmosphere and Ocean, University of Washington, Seattle, Washington, USA.
[3]NOAA Atlantic Oceanographic and Meteorological Laboratory, Miami, Florida, USA.

0148-0227/11/2010JC006910

to gaps in the spatial sampling coverage. Advection by mesoscale eddies, which have velocities that often greatly exceed the velocity of the time mean circulation, can change spatial distribution of floats even more significantly. The overall spatial coverage can be expected to become more uniform, which can improve reconstruction accuracy [*Kamenkovich et al.*, 2009a], but local effects can be more complicated. Finally, mesoscale variability in temperature and salinity results in strong background noise in the sampled profiles, which can lead to biases in the reconstructed fields, especially if only a small number of profiles are available. For example, it is well known that the standard error in a sample average of a random variable is expected to be $\sigma/n^{1/2}$, where σ is the standard deviation in the variable and n is the number of samples [e.g., *Leith*, 1973].

[5] The objective of this study is to analyze the mentioned effects of mesoscale variability on Argo-based reconstructions in an idealized, but relevant to the real ocean, setting. The study employs a suite of idealized OSSEs carefully designed to achieve this objective. These OSSEs are carried out in a North Atlantic model forced with the annual mean atmospheric forcing. The motivation behind the use of such idealized forcing is that it permits a straightforward isolation of the effects of mesoscale variability in the simulated fields and attribution of a part of reconstruction errors to these effects. The obvious limitation is that we can only investigate reconstruction errors of the annual mean state of the modeled ocean; however, it is an important step toward understanding the effects of mesoscale variability on the ability of profiling arrays to capture both the mean and temporal variability of ocean states. The article is organized as follows. The high-resolution general circulation model (GCM) is described in section 2 which also describes the sensitivity simulations. The results are presented in section 3 followed by the conclusions in section 4.

2. Numerical Model and Simulations

[6] The high-resolution numerical model used here has a spatial resolution of 1/8° in both latitudinal and longitudinal directions, which permits mesoscale eddies. The model parameters, forcing fields and simulated ocean state are all described by *Kamenkovich et al.* [2009b] and *Booth and Kamenkovich* [2008]. Here, we present only a brief description of the model.

[7] The numerical model is based on the GFDL MOM 3.0 code [*Pacanowski and Griffies*, 1999], which solves the equations of motion on fixed geopotential surfaces. The model domain extends from 14°N to 60°N and from 70°W to 10°W. The depth of the ocean is limited to 3000 m, and there are 30 vertical levels with thicknesses increasing away from the surface. Model topography is estimated from the 1° × 1° Scripps data set, which helps to accelerate convergence of the solution; see *Booth and Kamenkovich* [2008] for details.

[8] The model is set up in a way to produce the annual mean hydrography and circulation, which greatly simplifies the definition of eddies and analysis of their effects. The surface heat and freshwater fluxes have a form of restoring to the annual mean climatological values of the sea surface temperature and salinity, both derived from the high-resolution (1/4°) version 2 of the World Ocean Atlas 2005 [*Boyer et al.*, 2005]. The restoring time scales for temperature and salinity are 60 and 180 days (for a 50 m top layer), respectively. The annual mean zonal and meridional components of the surface wind stress are derived from the NCEP 1979–2001 reanalysis. The model solves for the explicit free surface evolution. Sponge boundaries, where the temperature and salinity are restored to the annual mean climatology with the time scale of 180 days, are employed at the northern and southern boundaries of the domain in order to mimic buoyancy exchanges with the ocean outside the model domain. Solid insulating walls are placed at the eastern and western boundaries and no-slip boundary conditions are used.

[9] Most of horizontal mixing of momentum, temperature and salinity is done by explicitly simulated mesoscale eddies. Small horizontal viscosity and diffusion is retained in the model in order to represent submesoscale mixing processes and for the sake of numerical stability–biharmonic horizontal viscosity and diffusivity are 10^{11} m^4 s^{-1} and 10^{10} m^4 s^{-1}, respectively; see also *Smith et al.* [2000] who use similar values. Vertical diffusion is kept to a realistically low value for the ocean far above rough topography, 10^{-5} m^2 s^{-1} [*Ledwell et al.*, 1993].

[10] The simulation of the annual mean stratification and circulation is discussed in detail by *Kamenkovich et al.* [2009b] and is only briefly summarized here. The pycnocline is somewhat shallower than the observed one, which is explained by the limited meridional extent of our domain. The simulated Gulf Stream has a realistic width of approximately 100 km, and it separates from the coast at around 35°N. The path of the eastward Gulf Stream extension is very unsteady and a part of the Gulf Stream quickly turns north and does not turn east until it reaches 40°N. All these problems are typical of many ocean models, even more comprehensive ones than ours [e.g., *Nakamura and Chao*, 2000]. The Labrador Current in the model is, however, concentrated and coherent. With the exception of the upper 200 m, the simulated time mean flow is dominated by multiple zonal jets, which have been detected in altimeter data [*Maximenko et al.*, 2005; *Huang et al.*, 2007]; float measurements [*Hogg and Owens*, 1999; *Treguier et al.*, 2003]; and eddy-resolving GCMs [*Galperin et al.*, 2004; *Nakano and Hasumi*, 2005; *Richards et al.*, 2006].

[11] The simulated eddy field exhibits a reasonable level of variance. The standard deviation of the sea surface height anomaly is shown in Figure 1b; the average values are comparable to the ones estimated from the AVISO satellite data (Figure 1a). The model, however, tends to underestimate the variance in the sea surface height in some parts of the domain, most likely due to the lack of synoptic component in the atmospheric forcing. Most notable differences are observed in the vicinity of the Gulf Stream extension, western part of the subpolar region (west of 40°W) and northeastern part of the subtropical region (east of 40°W).

[12] The Argo trajectories are calculated based on the daily snapshots of velocities, diagnosed from a 9 year run of the GCM. The simulations are run for 3240 days (9 years with 360 days each). The simulated Argo-like array of 243 floats is initially distributed uniformly in the model domain. All the floats are deployed on the same day and the number of floats remains constant throughout the experiment. In the “STANDARD” simulation, the floats are

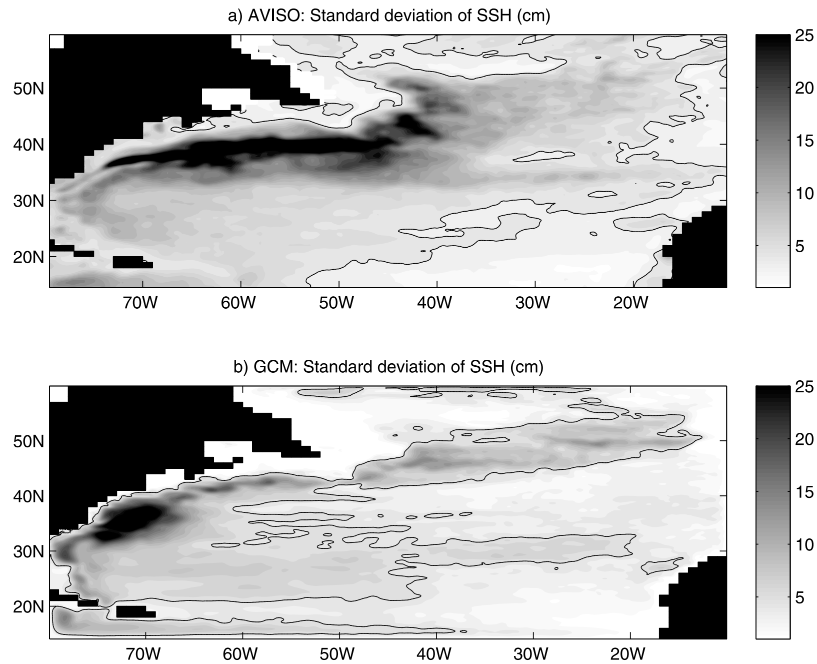

Figure 1. Eddies in the model and observations. Shown is the standard deviation of the sea surface height anomaly as calculated from (a) the 1992–2010 AVISO data set with climatological annual cycle removed (courtesy of Erik van Sebille) and (b) the 9 year simulation by the model used in this study. Units are given in cm; 10 cm contour is shown in black. Model topography is shown in black.

advected by the GCM-simulated velocities at 1500 m depth, when they are not at the surface and when the ocean is deep enough. The floats surface every 10 days, while taking an instantaneous vertical profile during their ascent, spend 8 h at the surface, where they are advected by the surface currents and then return to the 1500 m "parking" depth level. The ascent and descent are instantaneous, and the path is purely vertical, unlike in the real-life floats, which can be horizontally displaced during their ascent/descent. These displacements, together with errors in determining surfacing positions, introduce uncertainties in the locations and the profiles of the real-life Argo floats. Again, these uncertainties are beyond the scope of this study. The floats that enter a region shallower than 1500 m continue to take profiles in the model, whereas in reality some of such floats are damaged and are unable to continue the transmission of data. Between the profiles, such floats are advected by the deepest velocities at this location in this model. Note also that these idealized simulations do not attempt to account for the actual launch times and locations, differences in float design, instrumental errors, varying drift and profiling depths, and varying surface times.

[13] In addition to the STANDARD simulation, two sensitivity simulations aimed at isolating the effects of mesoscale eddy variability are performed. The velocities and temperature/salinity fields are modified in these simulations. As discussed in the Introduction, the mesoscale variability is expected to affect the reconstruction errors in two major ways: through rapid time-varying advection of the floats and through mesoscale variability in the sampled temperature and salinity fields. The sensitivity simulations are aimed at separating these two effects of eddies, which are defined here as deviations from the 9 year time mean. Note that such a most straightforward definition is only possible in an idealized model without an annual cycle and interannual variability. In the sensitivity simulation "MEAN_ADV" the Argo floats are advected by time mean velocities through the time-varying hydrographic field. In the simulation "MEAN" the eddy effects on both the velocity field and hydrography are removed by using the time-averaged fields. Comparisons between the STANDARD simulation and these two sensitivity simulations allow the separation of the two effects eddies have on the reconstructed fields.

3. Results

[14] Reconstructed fields of temperature, salinity, and zonal and meridional velocities are analyzed in this section. For the reconstruction of temperature and salinity, the results from the pseudo measurements are objectively analyzed by using the objective analysis (OA) scheme of *Mariano and Brown* [1992]. Gridded $1 \times 1°$ maps are produced at each 10 day sampling. A Gaussian correlation function with the e-folding scale of 3° in both latitude and longitude is assumed. The relative errors of the OA are defined as the ratios of estimated errors (variance of the estimator) over true data variance. In our analysis, all mapped data with relative errors larger than 0.85 are discarded and the data points flagged as "bad." The results are discussed in section 3.2, following the discussion of the float distribution in section 3.1.

[15] Surface and 1500 m zonal and meridional velocities are estimated from the difference in the float positions between the end and the beginning of their 8 h stay at the

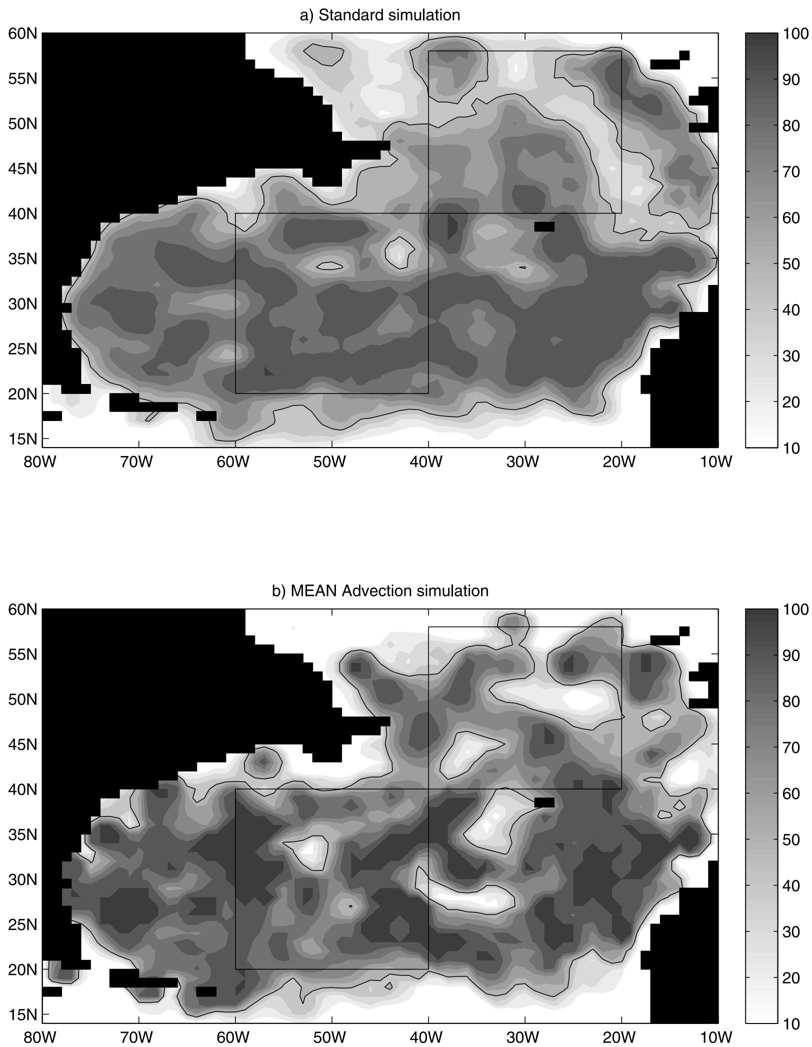

Figure 2. Sampling coverage by the simulated Argo array. Shown is the percentage of valid OA values (error less than 0.85) at each grid point at 1000 m depth during the 9 year lifespan of the simulated Argo system for (a) the STANDARD simulation and (b) the MEAN_ADV simulation. The contour represents 50% value. Land areas are shaded black. Also shown are the subtropical and subpolar gyre regions used for the analysis.

surface and the 232 h stay at the depth of 1500 m. Deep velocity values for floats that entered a shallow region are not used in the analysis. One of our main objectives is to determine how accurately a detailed structure in the horizontal velocity in general, and multiple zonal jets in particular, can be reproduced by the Argo-based reconstructions. For this reason, the resulting velocities are spatially averaged within 1° × 1° boxes and no coarse-grained spatial smoothing is done; coarser resolutions, however, are also analyzed in section 3.3. We found the averaging to lead to a good spatial resolution of oceanic fronts and to allow detection of the multiple zonal jets (see section 3.3). In calculating estimates of the time mean velocities, grid points with fewer than 5 points in time are excluded from the resulting velocity maps.

3.1. Distribution of Floats

[16] The spatial coverage changes significantly with time, due to the movements of the floats. As a result the coverage, initially nearly uniform, becomes nonuniform. Figure 2 illustrates these changes in the simulations, by showing the percentage of 10 day snapshots that produced valid OA values at each 1° × 1° cell with respect to the entire 9 year simulation. Excluded values at any time correspond to gaps in coverage and result in smaller values in Figure 2. Changes in the float distribution can be expected to be caused by both time mean and eddy advection, and will have an impact on the accuracy of the reconstruction of oceanic fields. The STANDARD and MEAN_ADV simulation help to investigate how important these two effects are.

[17] In both simulations most of the domain has a good spatial coverage with valid OA values at least half of the time (contour line in Figure 2). Areas with very poor coverage are, however, also clearly visible. They are located, for example, in the southernmost and northernmost parts of the domain, where during their stay at the surface, the floats are advected toward the center of the domain by Ekman

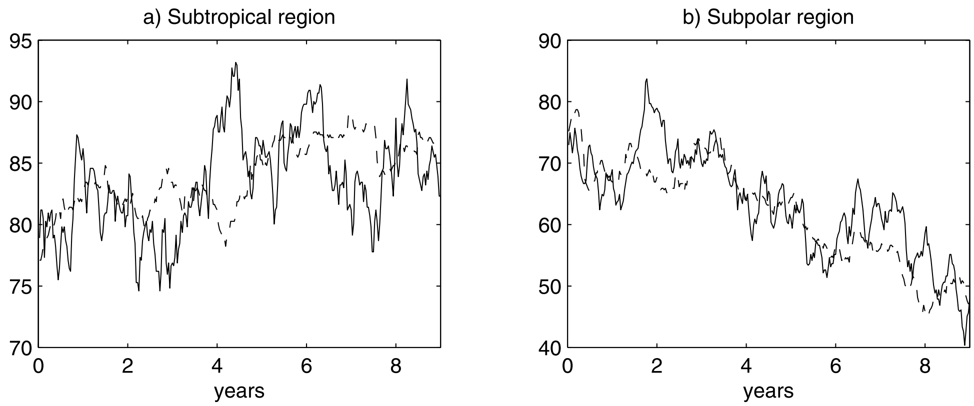

Figure 3. Time dependence in spatial coverage. The percentage of valid OA values as a function of time (years) at each 10 day sampling time step in the (a) subtropical and (b) subpolar box regions. The solid lines show the results for the STANDARD simulation, and the dashed lines show the results for the MEAN_ADV simulation.

velocities. These factors lead to the eventual absence of floats in the vicinity of these boundaries. Therefore, these regions are not included in the analysis. Other areas with poor coverage are located north of the Gulf Stream (around 40°N), west of the North Atlantic Ridge, over the western part of the subpolar gyre, and in the region 45°N–55°N 30°W–20°W.

[18] Despite these similarities, the spatial distribution of the sampling coverage is substantially different between the two simulations. In particular, the gaps in coverage increase substantially in both the subtropical and subpolar gyres if no eddies are present (Figure 2b). Therefore it is clear, that the eddies act to produce more uniform spatial coverage in these regions. In particular, the western boundary region north of

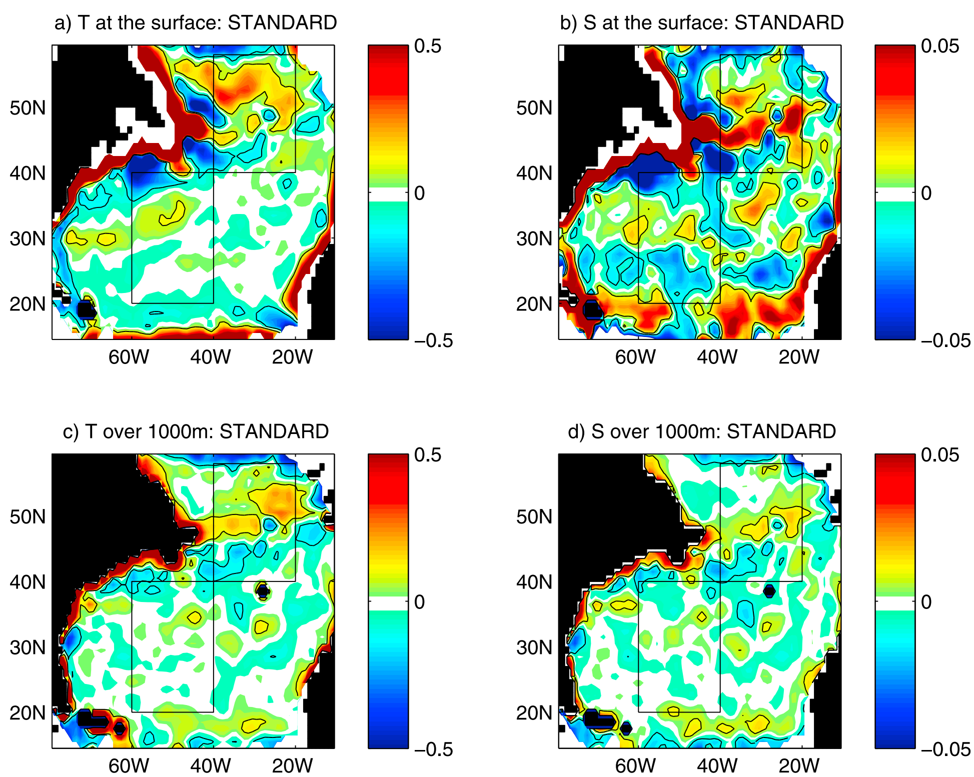

Figure 4. Reconstruction errors for (a and c) temperature (units are in °) and (b and d) salinity (units are given in psu) in the STANDARD simulation. Figures 4a and 4b show the surface values; Figures 4c and 4d display values averaged over the top 1000 m. The contour interval for temperature is 0.05 K; and the contour interval for salinity is 0.005 psu. The contour lines show the ±0.1 K line for temperature and ±0.01 psu for salinity. Also shown are the subtropical and subpolar gyre regions used for the analysis. Topography is shown at the surface for Figures 4a and 4b and at 1000 m depth for Figures 4c and 4d. Areas with insufficient coverage are left blank.

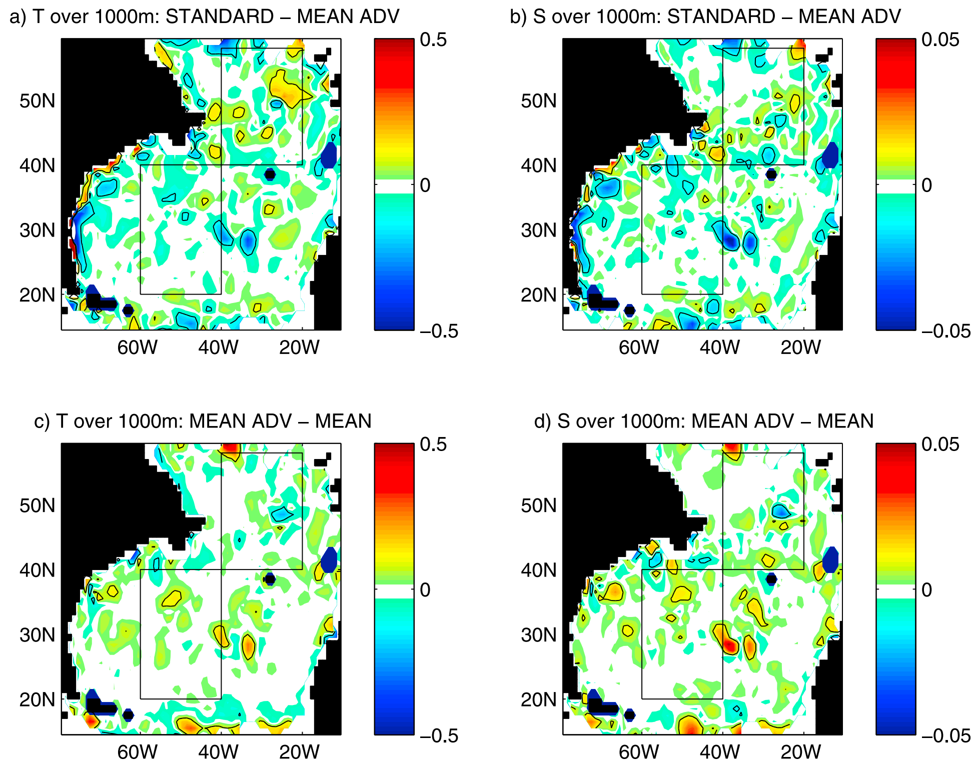

Figure 5. Effects of the mesoscale variability on the reconstruction errors in the temperature and salinity averaged over the upper 1000 m. The differences between the absolute values of the reconstruction errors between the STANDARD and MEAN_ADV simulation for (a) temperature and (b) salinity and the differences between the absolute values of the reconstruction errors between the MEAN_ADV and MEAN simulations for (c) temperature and (d) salinity are shown. The contour interval for temperature is 0.05 K; and the contour interval for salinity is 0.005 psu. The contour lines show the ±0.1 K line for temperature and ±0.01 psu for salinity. Also shown are the subtropical and subpolar gyre regions used for the analysis. Topography is shown at 1000 m depth. Areas with insufficient coverage are left blank.

35°N, the region around the North Atlantic Ridge, and the interior of the subpolar gyre all exhibit noticeably better spatial coverage in the STANDARD simulation. The southern part of the Labrador Current (south of 55°N) and its eastward extension, in contrast, both have a significantly improved coverage in MEAN_ADV, which can be explained by the absence of the eddy-driven dispersion of the floats in this simulation. This is consistent with *Booth and Kamenkovich* [2008], who concluded that eddies tend to remove passive tracers from this current.

[19] To analyze the changes in the coverage over time in more detail, we choose two regions (shown in Figure 2): one with slowly increasing and one with decreasing average coverage. Note that these changes in the average coverage can only be due to the floats leaving/entering these regions, as the total number of floats in the entire domain is constant in these idealized simulations. In the first region, located in the subtropical gyre ("subtropical box"), the number of floats increases from 46 to 59 in the STANDARD simulation, and to 68 in the MEAN_ADV simulation (not shown). Mean advection, therefore, brings more floats to this region, whereas the eddy field acts to remove them. This noticeable increase in the number of floats in time is, however, accompanied by developing gaps in coverage, and the net result in the subtropical box is a very modest increase in the percentage of valid OA points. The annual mean ratio between the number of valid OA values to the total number of OA values increases from 80.5% to 86.5% (86%) for the STANDARD (MEAN_ADV) simulations, and there is no significant trend (Figure 3a). Higher variability in this ratio in the STANDARD simulation also suggests that the eddies cause a noticeable portion of the variability in the coverage.

[20] In the second region, located in the subpolar gyre ("subpolar box"), the coverage steadily deteriorates with time. The total annual mean number of floats steadily decreases from 30 to 24 (23) in the STANDARD (MEAN_ADV) simulations over the 9 years, due to more floats leaving than entering this region. The decrease in the number of floats, combined with the developing gaps in coverage, results in a noticeable downward trend in the percentage of valid OA values that corresponds to a decrease by from 70% to 50% (71% to 49%) in the STANDARD (MEAN_ADV) simulations (Figure 3b). The decreasing spatial coverage in the subpolar region is clearly a result of the mean advection, and the effects of eddies are nearly negligible. Variability range in the detrended values in Figure 3b is very similar between the two simulations.

3.2. Temperature and Salinity

[21] Reconstruction errors are defined here as the difference between the reconstructed fields and the actual model simulated values. To make this definition of reconstruction

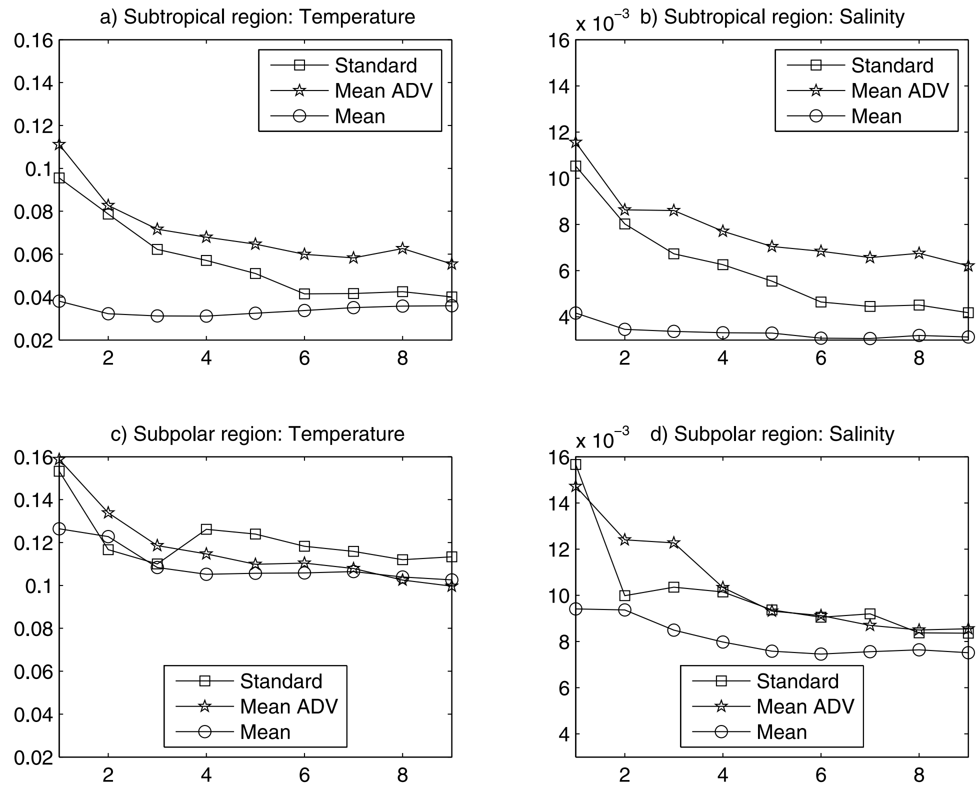

Figure 6. RMS reconstruction errors for the time mean (a and c) temperature and (b and d) salinity, averaged over 1000 m, as a function of the averaging period in years. The values are shown for the subtropical (Figures 6a and 6b) and the subpolar (Figures 6c and 6d) regions.

errors most meaningful, the model-simulated data are averaged within 1° × 1° bins and smoothed by the Guasian filter with the 3° e-folding scale in both latitude and longitude. Both the differences of the surface values and the values averaged over the upper 1000 m are analyzed herein. Due to the absence of the seasonal cycle in the idealized GCM used for this study, we restrict our analysis to the 9 year climatological means in all fields. Only valid OA values are used for calculating the climatology derived from the simulated float profiles.

[22] The reconstruction errors in the climatology of temperature and salinity are shown in Figure 4 for the STANDARD simulation, for both the surface and the depth-averaged values (over the upper 1000 m). In most of the subtropical gyre, the reconstruction errors are small and do not exceed 0.1 K for temperature both at the surface and in the depth average. Depth-averaged salinity biases in the subtropical gyre are typically less than 0.01 psu. The reconstruction errors are larger at the surface, but typically smaller than 0.02 psu. In the subpolar region, the reconstruction errors are noticeably larger than in the subtropical region. Surface temperatures exhibit significant positive biases in the interior of the subpolar gyre, which can be as high as 0.25 K. Reconstruction errors in the depth-averaged temperatures are smaller than at the surface, but even they exceed 0.2 K in some parts of the subpolar gyre. Surface salinities exhibit a very large (greater than 0.05 psu) positive bias along the eastward extension of the Labrador Current, where it becomes a part of the North Atlantic Current in the model, and the negative bias immediately south from it. These biases in the Labrador Current extension can be explained by the difficulty of the sparse coverage per design (one float every 3° × 3° initially) to resolve local minima and strong gradients in temperature and salinity, resulting from the advection of relatively cold and fresh subpolar waters by the Labrador Current. Note that the reconstruction errors would be significantly larger, if they were calculated from the actual, unsmoothed model fields. The reconstruction errors are further enhanced by the poor coverage in this region (Figure 2a) and can also be influenced by mesoscale eddies, whose effects are analyzed next.

[23] When the effects of eddy advection on float trajectories are removed in the MEAN_ADV simulation, the resulting changes in the reconstruction errors are complex (Figure 5). Careful analysis of Figures 2, 4, and 5 demonstrates that the sampling coverage alone cannot explain the difference in reconstruction errors between the two simulations. As discussed in section 3.1, spatial sampling density becomes less evenly distributed in the absence of mesoscale eddies in most of the domain. As a result, gaps in the coverage are larger in the MEAN_ADV when compared to the STANDARD simulation, which corresponds to the increased reconstruction errors in several parts of the domain, including 28°N, 30°–40°W or 35°N, 55°W. On the other hand, the western boundary region 25°N–32°N exhibits improved coverage and smaller reconstruction errors in MEAN_ADV, relative to the STANDARD simulation (positive values in Figure 5).

[24] In other parts of the domain, the difference between the STANDARD and MEAN_ADV simulations cannot be explained by the difference in the sampling coverage. Most

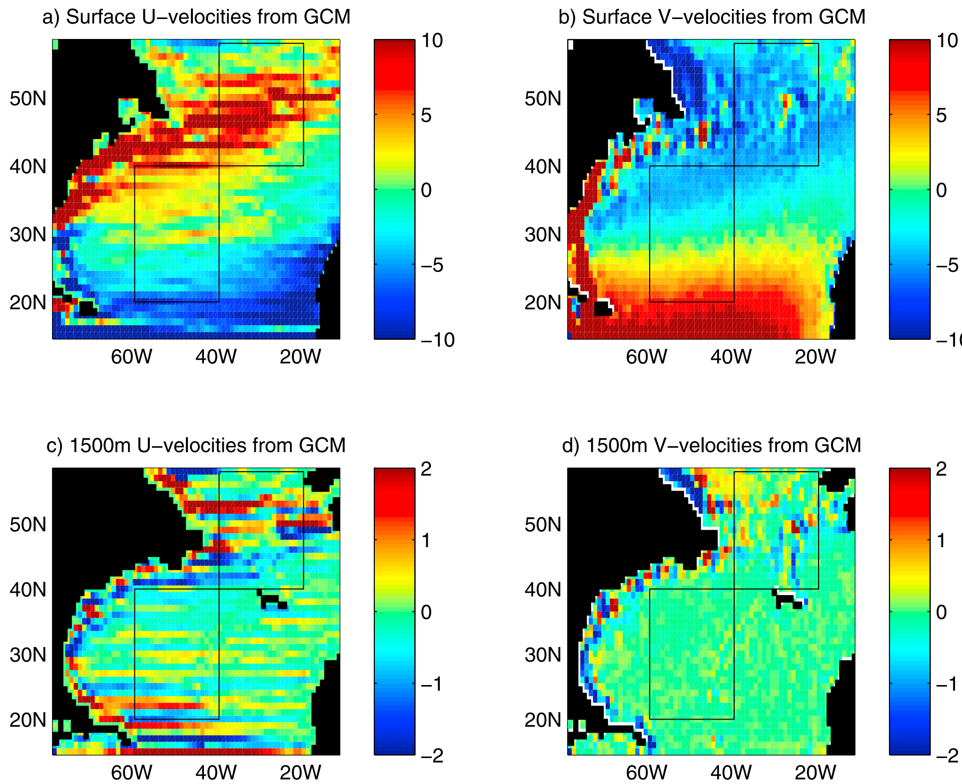

Figure 7. GCM-simulated time mean velocities: (a) zonal velocities at the surface, (b) meridional velocities at the surface, (c) zonal velocities at 1500 m depth, and (d) meridional velocities at 1500 m depth. Box regions for zonal averaging are also shown. Units are given in 10^{-2} m s^{-1}. Topography is shown at the surface in Figures 7a and 7b and at the 1500 m depth in Figures 7c and 7d.

notably, the reconstruction errors are significantly smaller in the absence of eddies near 50°N, 25°W which can be seen as a positive difference between the errors of the STANDARD and MEAN_ADV cases (Figure 5a), in contrast with the coverage gap in MEAN_ADV. Within the Labrador Current (around 50°N), the reconstruction errors are larger in the absence of mesoscale eddies, which is reflected in a negative difference of the errors from the STANDARD and MEAN_ADV simulations. This area, however, has better sampling coverage in the MEAN_ADV simulation (Figure 2).

[25] The spatial correlation between the difference in the spatial coverage in STANDARD and MEAN_ADV (between the fields in Figures 2a and 2b) and the corresponding difference in reconstruction errors (Figure 5a) is approximately −0.2 (negative correlation means that errors decrease with better coverage). This relatively low correlation is not as surprising as it appears. Low spatial coverage corresponds to a large number of "bad" reconstructed values, which are discarded at each 10 day snapshot. However, a small number of values in the immediate vicinity of the location can lead to more accurate reconstruction than a large number of values farther away, especially if the temporal variability in this location is low. As our analysis shows, this is the case, for example, in the Labrador Current (around of 50°N, see also Figure 1b).

[26] The importance of the mesoscale variability of the temperature and salinity field for the reconstruction errors is addressed in the "MEAN" simulation, in which the floats are advected by the time mean currents (as they are in the MEAN_ADV simulation). In addition, the variability is removed from the temperature and salinity fields. The difference between the reconstruction errors for the MEAN_ADV and MEAN simulations is, therefore, explained by the presence of the mesoscale variability in the hydrographic fields of the former simulation, as the float positions are identical for these two simulations. Throughout most of the domain the reconstruction errors in the MEAN simulation are smaller than in the MEAN_ADV simulation (Figures 5c and 5d). Most notably, the reconstruction errors at 28°N, 30°W–40°W are substantially reduced with the removal of variability from temperature and salinity. Therefore, the errors in this location in the MEAN simulation become in fact similar to those in the STANDARD simulation. Large reconstruction errors in this location in the MEAN_ADV simulation are explained by low spatial coverage (Figure 2b) combined with high mesoscale variability (Figure 1b), which means that the removal of the variability reduces the errors.

[27] In order to analyze the dependence of the reconstruction accuracy on the lifetime of the simulated Argo system, we computed the reconstruction errors for varying durations of the sampling: from 1 to 9 years. These dependencies are calculated in the two regions selected above and for both the time mean temperature and salinity. The reconstruction errors are shown as the square root of the area-averaged squared errors in the time mean depth-averaged fields (root mean square (RMS) error) in Figure 6.

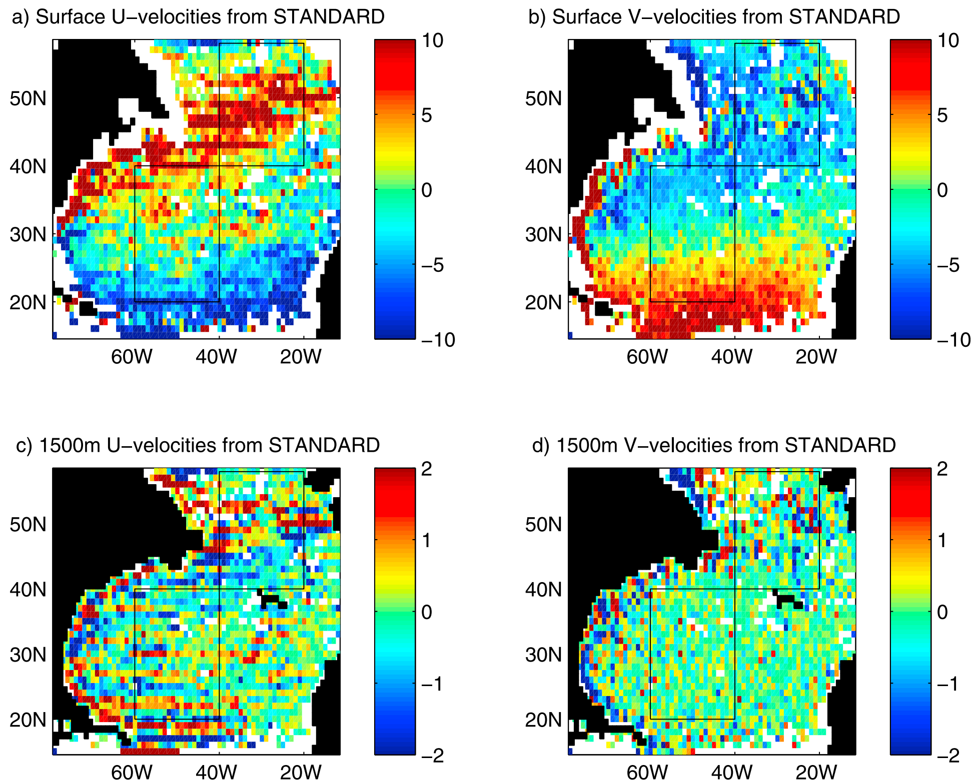

Figure 8. Time mean velocities reconstructed from the float trajectories in the STANDARD simulation: (a) zonal velocities at the surface, (b) meridional velocities at the surface, (c) zonal velocities at 1500 m depth, and (d) meridional velocities at 1500 m depth. Box regions for zonal averaging are also shown. Units are given in 10^{-2} m s^{-1}. Locations with fewer than five data points (over the 9 year period) are masked (white). Topography is shown at the surface in Figures 8a and 8b and at the 1500 m depth in Figures 8c and 8d.

[28] In the STANDARD simulation, the subtropical region exhibits a gradual decrease in the reconstruction errors with increasing averaging period, the RMS error is more than halved from year 1 to year 9, both for temperature and salinity (Figures 6a and 6b). In the subpolar region (Figures 6c and 6d), the situation is more complicated due to the gradual loss of sampling coverage caused by floats leaving this region (Figure 3b). Initially, the reconstruction errors decrease with time (Figures 6c and 6d), but for the averaging period longer than 3 years, the reduction in the RMS error slows down. These results agree well with the fact that the coverage does not change significantly in the first about 3 years (Figure 3b). As a result, the subpolar RMS error for the 9 year duration of the STANDARD simulation significantly exceeds the subtropical RMS error by almost a factor of 3 for temperature and by almost a factor of 2 for salinity.

[29] Although in both regions the RMS errors decrease steadily with time in the MEAN_ADV simulation, the effects of the mesoscale eddy advection vary between the two regions. In the subtropical region, the RMS errors in the MEAN_ADV simulation always exceed the RMS errors in the STANDARD simulation, which is due to the gaps in coverage that develop in the MEAN_ADV case. In contrast to this, in the subpolar region, the RMS error in MEAN_ADV is smaller than in the STANDARD case for temperature, for periods longer than 4 years.

[30] The RMS error in the MEAN simulation starts at a lower value and changes very little with the increasing duration of the Argo observations. As a result, the adverse effects of the mesoscale variability in temperature and salinity on the reconstruction accuracy, estimated by the difference between MEAN_ADV and MEAN values of the RMS error, are the strongest for shorter duration of the Argo observations. In particular, the RMS error in the subtropical region in the MEAN_ADV simulation is more than twice as large as in the MEAN simulation for the first 4 years, which is due to the presence of the mesoscale variability in temperature/salinity in the former case.

[31] The standard error of a true random variable is expected to decrease with the number of sampling n as $n^{-1/2}$; see Introduction. We describe the decrease rate by $1/n^{a}$, where the parameter a can be estimated by

$$a = -\log\left(\frac{\sigma(T)}{\sigma(1)}\right)(\log T)^{-1}, \qquad (1)$$

where $\sigma(T)$ is the RMS error as a function of the duration of measurements in years T. For a true random variable the parameter a is 0.5. Our analysis shows that the decrease in the RMS error with the longer averaging period is noticeably slower, in the case of our simulated Argo array. For the analysis, we calculate the parameter a for the values of T from years 2 to 9, together with its time-averaged value over

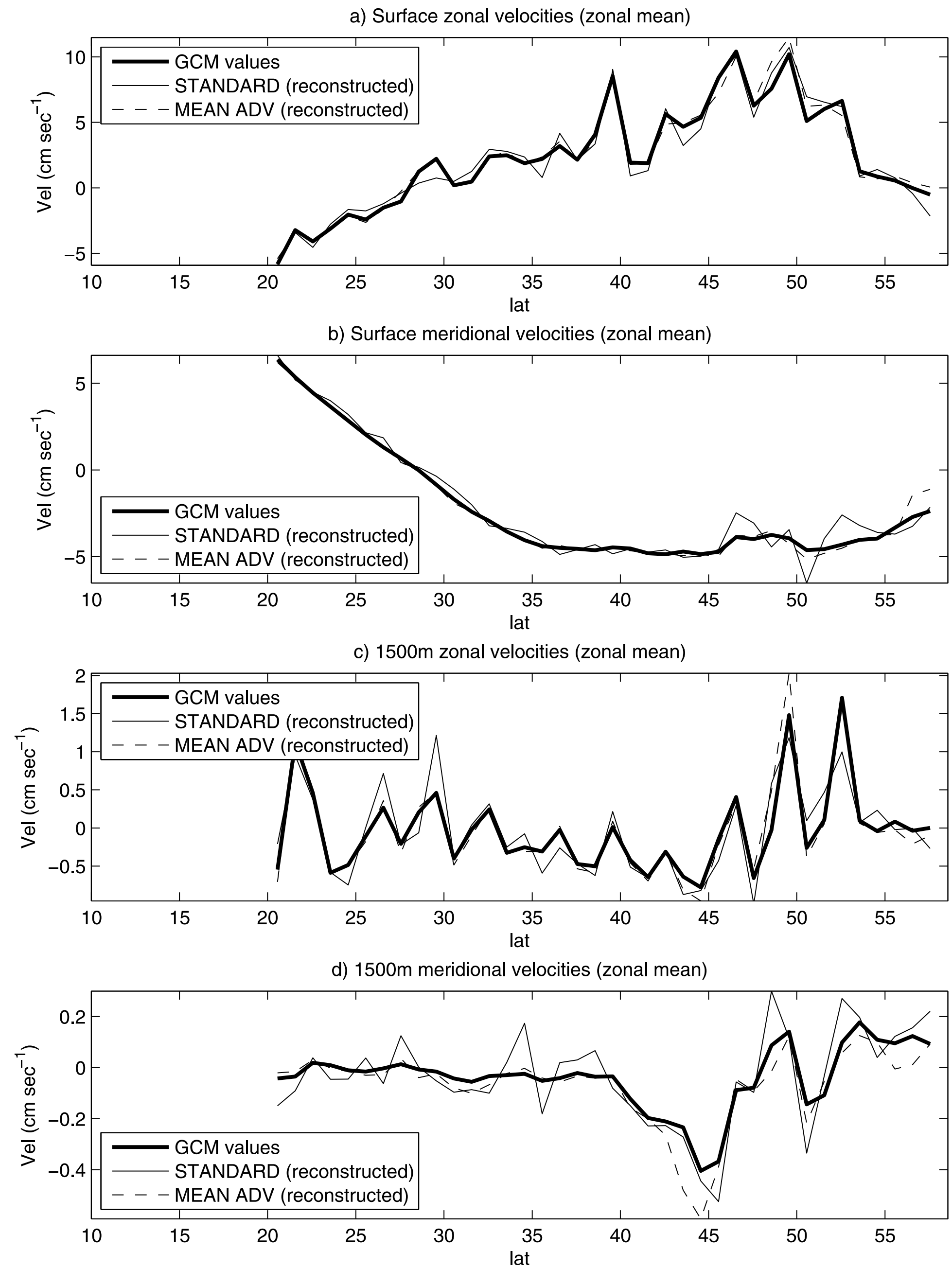

Figure 9. Argo-based reconstruction of zonally averaged velocities. Velocities zonally averaged within the two box regions (subtropical south of 42°N, subpolar north of 42°N): (a) zonal velocities at the surface, (b) meridional velocities at the surface, (c) zonal velocities at 1500 m depth;, and (d) meridional velocities at 1500 m depth. GCM values (thick solid line) and two reconstructions, STANDARD (thin solid line) and MEAN_ADV (dashed line), are shown.

9 years and its deviation from this time mean value. When the deviation is greater than the mean value itself, the parameter *a* is assumed undefined. For the subtropical gyre region, both temperature and salinity correspond to a mean parameter *a* of 0.3–0.35 for both the STANDARD and the MEAN_ADV simulations. In the subpolar region, the mean parameter *a* is even smaller and equals to 0.2–0.25 in the MEAN_ADV simulation; it is undefined for the STANDARD simulation. For the MEAN simulation the parameter *a*, and thus the decrease rate, is undefined in both regions.

3.3. Results: Horizontal Velocities

[32] Our main objective here is to determine how accurately horizontal velocities can be estimated from Argo trajectories. In particular, we are interested in the possibility that such estimates can detect multiple zonal jets–flow patterns recently discovered in satellite data and in com-

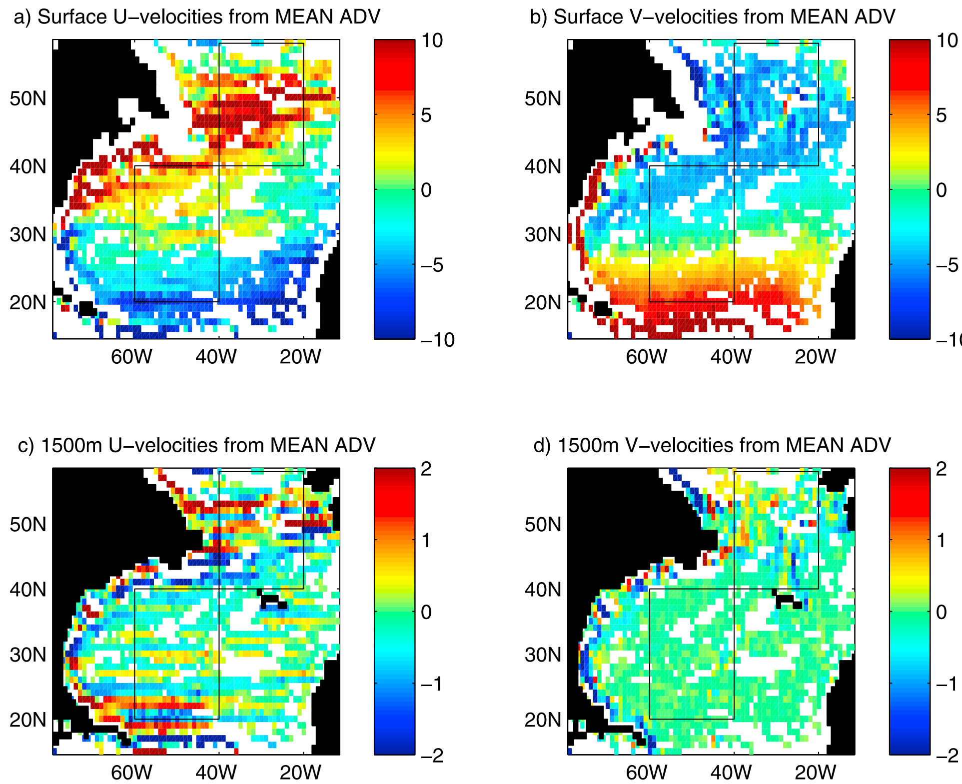

Figure 10. Time mean velocities reconstructed from the simulated float trajectories in the MEAN_ADV simulation: (a) zonal velocities at the surface, (b) meridional velocities at the surface, (c) zonal velocities at 1500 m depth, and (d) meridional velocities at 1500 m depth. Box regions for zonal averaging are also shown. Units are given in 10^{-2} m s^{-1}. Locations with fewer than five data points (over the 9 year period) are masked (white). Topography is shown at the surface in Figures 10a and 10b and at the 1500 m depth in Figures 10c and 10d.

prehensive high-resolution ocean models [*Galperin et al.*, 2004; *Maximenko et al.*, 2005].

[33] For a valid comparison with the trajectory-based velocity estimates, the high-resolution GCM-simulated values are averaged within the same 1° × 1° boxes as the trajectory-based estimates (Figure 7). Alternating zonal jets are most clearly seen in the deep zonal velocities in our model (Figure 7c; see also *Kamenkovich et al.* [2009b] for more detail), since the large-scale mean currents are weaker at this depth. At the surface, the powerful large-scale gyre circulation masks the jets (Figure 7a). In the model, the characteristic width of these jets is 1.5–2°, and the peak velocities exceed 0.05 m s^{-1}. Note that the 1° × 1° spacing allows only marginal resolution of the jets. Attempts to achieve higher spatial resolution in the velocity reconstruction (0.5° × 0.5°) are not presented here because they led to very noisy fields and very large reconstruction errors.

[34] The banded patterns in the zonal velocities seen in the trajectory-based estimates are similar to the GCM-simulated currents, but noisier (Figures 7 and 8). At the surface, eastward jets, masked by the eastward large-scale currents, can be seen as local maxima in zonal velocities between 25°N and 55°N, but most clearly pronounced north of 40°N. At the 1500 m depth of the floats, the zonal jets can be detected in the reconstructed velocities everywhere south of 55°N (Figure 8c). The Argo-reconstructed velocities in these jets are, however, highly spatially variable and tend to be larger than the actual GCM values in the middle of the subtropical gyre. North of 55°N, the coverage with floats is not sufficient to result in valid velocity estimates.

[35] To illustrate the agreement between the zonal jet structure from the GCM and the simulated floats, zonally averaged zonal velocities are shown in Figures 9a and 9c for GCM values (blue lines) and their Argo-based reconstructions (green and red lines). The zonal boundaries for the averaging are given by the extents of the subtropical and subpolar boxes. Multiple minima and maxima in the reconstructed and actual velocities, corresponding to the jets, align very well at both the surface and at depth. The local reconstruction errors (not shown), however, are noisy and can be large. Stricter requirements on the minimum number of data points act to reduce the errors at the expense of significantly deteriorated spatial coverage.

[36] The reconstruction of the meridional velocities appears to be less accurate than the reconstruction of zonal velocities, especially north of 45°N at the surface (Figure 9b). Small-scale anomalies in the meridional velocities are not captured by the trajectory-based estimates. When compared with the signal, the errors are particularly large at depth, where the reconstructed velocities are very noisy and the actual velocities are very weak. Large-scale meridional currents at the surface are, however, represented reasonably well in the subtropical gyre, which is illustrated by the zonally averaged meridional velocities (Figures 9b

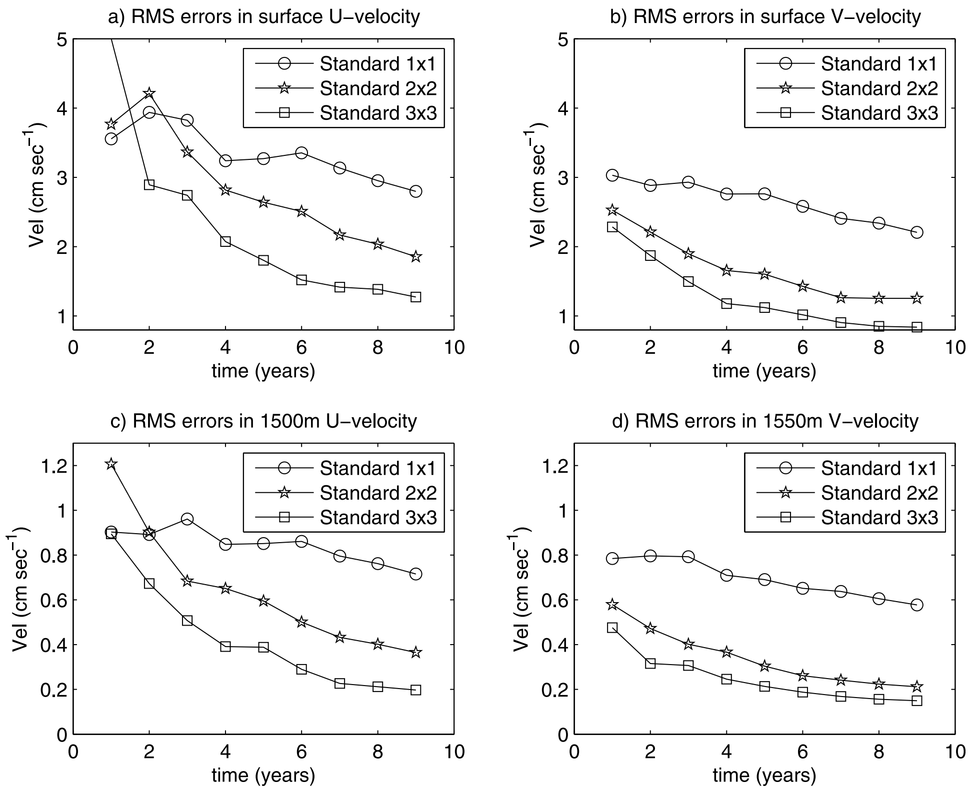

Figure 11. RMS reconstruction errors of the time mean velocities in the STANDARD simulation, area averaged over the area covered by the subtropical and subpolar box regions. Values are shown as a function of the averaging period (in years) for three grid sizes: 1° × 1° (circles), 2° × 2° (stars), and 3° × 3° (squares). (a) Zonal velocities at the surface, (b) meridional velocities at the surface, (c) zonal velocities at 1500 m depth, and (d) meridional velocities at 1500 m depth.

and 9d). This result suggests that, in the gyre interior, it is possible to reconstruct the zonally integrated surface meridional volume (and possibly heat) fluxes, but not the detailed structure in the meridional velocities. At depth, the reconstruction of the meridional velocities appears to be largely unreliable at this resolution, mostly because the absolute velocities are so small.

[37] A large part of the errors in reconstruction of the velocities is caused by eddy advection. In the absence of the mesoscale eddies in the MEAN_ADV simulation, the accuracy of the velocity estimates is significantly improved at most locations, but the data coverage deteriorates at the same time (Figure 10). In fact, valid surface velocity estimates are not available in approximately 30% of grid points (up from 9% in STANDARD). The reconstruction of the zonally averaged (within the box regions) velocities improves dramatically in the subtropical gyre, but significant errors persist in the southern half of the subpolar gyre (Figures 9a and 9c). These errors are, however, mostly caused by the increased spatial gaps in the velocity estimates in the MEAN_ADV simulation. This is true, for example, near 49°N, where the reconstruction errors in the MEAN_ADV simulation are larger than in the STANDARD simulation. The reconstruction of the zonal mean of the meridional velocities at the surface is markedly improved in MEAN_ADV relative to the STANDARD simulation, due to the absence of eddies in the former case.

[38] Reconstruction errors decrease with the increased data coverage and with coarser resolution. This can be seen in Figure 11, which shows the RMS error of the velocities as a function of the duration of the observations and for the three different grids in the STANDARD simulation: 1° × 1°, 2° × 2° and 3° × 3°. In general, the RMS error in zonal velocity decreases more rapidly with time than for the meridional velocity and for coarser resolution than for the finer ones. While the decrease in the RMS error with averaging duration for the 1° × 1° grid cannot be described by the decrease rate of $1/n^a$, coarser resolutions are more consistent with this formula. The decrease tends to be slower than $1/n^{1/2}$ for the 2° × 2° grid, since the mean parameter a, as defined by (1) for the surface and deep velocities in meridional and zonal directions, is between 0.3 and 0.4. For the 3° × 3° grid, the decrease is faster, and a is 0.6 (0.4–0.5) for the zonal (meridional) velocities. The decrease in the RMS error is more rapid when going from 1° × 1° to 2° × 2° resolution than for the 2° × 2° to 3° × 3° resolution transition, especially for the meridional velocities.

4. Discussion and Conclusions

[39] This study analyzes the effects of mesoscale variability on the expected accuracy of an observing system with profiling floats, using idealized high-resolution simulations in the North Atlantic, without seasonal and interan-

nual variability in the surface forcing. The primary objective of this study is to explore the main effects of mesoscale eddies on the Argo observing system. Two main effects of the eddy variability are analyzed: eddy advection of the profiling floats and mesoscale variability in the sampled temperature and salinity fields. These effects are separated in two sensitivity simulations, in which first the eddy advection and then hydrographic variability is removed from the sampled fields. In both of the sensitivity simulations, the floats are advected by the time mean currents. The study focuses on the resulting changes in the sampling spatial coverage and on the accuracy of the reconstruction of temperature, salinity and horizontal velocities. Reconstruction of all these fields is significantly affected by the presence of mesoscale eddies.

[40] The effects of the eddy advection on the float distribution are complex. In some regions, such as the Labrador Current and its extension, eddies cause dispersion of the floats and a decrease in the spatial coverage. In other regions, such as the interior of the subtropical gyre, eddies help to distribute the floats more evenly, acting to reduce gaps in the spatial coverage. Identification of regions corresponding to strong eddy dispersion, based on Argo float trajectories, appears to be important, since these will require continuing redeployment of the floats.

[41] Gaps in the sampling coverage do not always correspond to elevated reconstruction errors, as demonstrated by the analysis of the simulations with and without eddies. In some parts of the domain, for example, poorer data coverage coincides with smaller reconstruction errors. It is clear that the data coverage alone cannot explain better reconstruction accuracy, and our analysis demonstrates that even a small number of very accurate samplings can result in accurate reconstruction of climatology, especially if the mesoscale variability at this location is low. Other factors, such as movement of the floats and under-resolved oceanic fronts and gradients can also play a role. Movements of floats by mesoscale eddies do not represent a major source of errors in most of the domain.

[42] In these idealized simulations, the variability of temperature and salinity is dominated by the mesoscale effects, since the surface forcing is lacking a seasonal cycle and interannual variability. The importance of the mesoscale variability is, therefore, conveniently isolated, which is only possible in an idealized study like this one. The effects of this mesoscale eddy “noise” on temperature and salinity are generally small for the reconstructions of the 9 year time means. The importance of the mesoscale variability increases for lower data coverage and shorter averaging period. For example, for the averaging period shorter than 3 years, the mesoscale variability in the temperature/salinity is the major source of reconstruction errors in the subtropical gyre. The errors are gradually reduced, when longer periods and larger number of samples are used; the reduction is, however, significantly slower than that for the standard error in a sample average of a random variable.

[43] Velocity estimates from the simulated Argo float trajectories at $1° \times 1°$ grid are accurate enough for detection of concentrated oceanic currents like the multiple zonal jets with characteristic widths of 1.5–2°. Zonal jets derived from the simulated Argo floats have a spatial structure that is in a good agreement with the actual GCM currents. The reconstruction errors are still large at some locations, but are significantly smaller in the zonal averages. The reconstruction errors are also noticeably smaller in $2° \times 2°$ and $3° \times 3°$ estimates, at the cost of the reduced resolution. Mesoscale variability in the velocities, as expected, introduces a significant source of reconstruction errors. The ability of the Argo-based velocity estimates to reconstruct the shape and positions of the zonal jets is, however, encouraging and can be used for the jet detection with the real Argo (such as in *van Sebille et al.*’s [2011] study).

[44] Meridional velocities are weak and noisy in the gyre interior, and the local estimates of the meridional velocities are not very reliable, since the reconstruction errors overwhelm the signal. The reconstruction errors are smaller in the estimates of the zonally averaged meridional velocities in the interior, and these estimates may provide valuable information for studies of the meridional overturning. Large reconstruction errors and gaps in coverage within western boundary regions, however, make estimates of the total Atlantic meridional overturning challenging, if based on the Argo trajectories alone.

[45] This study focuses on the most fundamental effects of eddies on the reconstruction accuracy of the climatological means in temperature, salinity and horizontal velocities. Estimates of the means are essential for the accurate detection of the variability in these fields. The effects of eddies on the accuracy of Argo-based reconstructions can, however, be expected to be even more significant in the real ocean. Reconstruction of the variability in the oceanic fields, arguably the most important stated task of the Argo array, is generally more challenging than the reconstruction of climatological annual mean [*Kamenkovich et al.*, 2009a]. In particular, gaps in coverage may lead to potentially more serious biases in the reconstructed fields due to seasonal and interannual variability in these fields. Mesoscale eddies in this model tend to be weaker than those observed in nature in some parts of the domain, and their effects can potentially be underestimated in this study. Additionally, small-scale eddies and high-frequency (shorter than 1 day) fluctuations, which are not included in this study, can also have a potential impact. The importance of mesoscale variability, and its potential interaction with variability on longer and shorter scales, calls for the comprehensive evaluation of these effects in more realistic OSSEs, which are currently under way. The results from this study can be used to interpret such simulations and to improve our understanding of what we can learn from the real Argo observation system.

[46] **Acknowledgments.** The authors would like to thank E. S. Sarachik, F. Bryan, and anonymous reviewers for their helpful advice on the analysis discussed in this manuscript. Kamenkovich and Cheng were supported by the NOAA Climate Program Office, Climate Observation Division; Kamenkovich would also like to acknowledge the support by NSF grants OCE 0346178 and 0749722.

References

Arnold, C. P., Jr., and C. H. Dey (1986), Observing-system simulation experiment: Past, present and future, *Bull. Am. Meteorol. Soc.*, *67*, 687–695, doi:10.1175/1520-0477(1986)067<0687:OSSEPP>2.0.CO;2.

Ballabrera-Poy, J., E. Hackert, R. Murtugudde, and A. J. Busalacchi (2007), An observing system simulation experiment for an optimal moored instrument array in the tropical Indian Ocean, *J. Clim.*, *20*, 3284–3299, doi:10.1175/JCLI4149.1.

Barth, N., and C. Wunsch (1990), Oceanographic experiment design by simulated annealing, *J. Phys. Oceanogr.*, *20*, 1249–1263, doi:10.1175/1520-0485(1990)020<1249:OEDBSA>2.0.CO;2.

Bennett, A. F. (1990), Inverse methods for assessing ship-of-opportunity networks and estimating circulation and winds from tropical expendable bathythermograph data, *J. Geophys. Res.*, *95*, 16,111–16,148, doi:10.1029/JC095iC09p16111.

Booth, J., and I. Kamenkovich (2008), Isolating the role of transient mesoscale eddies in mixing of a passive tracer in an eddy resolving model, *J. Geophys. Res.*, *113*, C05021, doi:10.1029/2007JC004510.

Boyer, T., S. Levitus, H. Garcia, R. Locarnini, C. Stephens, and J. Antonov (2005), Objective analyses of annual, seasonal, and monthly temperature and salinity for the World Ocean on a 0.25 degree grid, *Int. J. Climatol.*, *25*, 931–945, doi:10.1002/joc.1173.

Galperin, B., H. Nakano, H. Huang, and S. Sukoriansky (2004), The ubiquitous zonal jets in the atmospheres of giant planets and Earth's oceans, *Geophys. Res. Lett.*, *31*, L13303, doi:10.1029/2004GL019691.

Griffa, A., A. Molcard, F. Raicich, and V. Rupolo (2006), Assessment of the impact of TS assimilation from Argo floats in the Mediterranean Sea, *Ocean Sci.*, *2*, 237–248, doi:10.5194/os-2-237-2006.

Hackert, E. C., R. N. Miller, and A. J. Busalacchi (1998), An optimized design for a moored instrument array in the tropical Atlantic Ocean, *J. Geophys. Res.*, *103*, 7491–7509, doi:10.1029/97JC03206.

Hernandez, F., P.-Y. Le Traon, and L. H. Barth (1995), Optimizing a drifter cast strategy with a genetic algorithm, *J. Atmos. Oceanic Technol.*, *12*, 330–345, doi:10.1175/1520-0426(1995)012<0330:OADCSW>2.0.CO;2.

Hogg, N., and B. Owens (1999), Direct measurement of deep circulation within the Brazil basin, *Deep Sea Res.*, *46*, 335–353, doi:10.1016/S0967-0645(98)00097-6.

Huang, H.-P., A. Kaplan, E. Curchitser, and N. Maximenko (2007), The degree of anisotropy for mid-ocean currents from satellite observations and an eddy-permitting model simulation, *J. Geophys. Res.*, *112*, C09005, doi:10.1029/2007JC004105.

Kamenkovich, I., W. Cheng, E. S. Sarachik, and D. E. Harrison (2009a), Simulation of the Argo observing system in a global ocean model, *J. Geophys. Res.*, *114*, C09021, doi:10.1029/2008JC005184.

Kamenkovich, I., P. Berloff, and J. Pedlosky (2009b), Role of eddy forcing in the dynamics of multiple zonal jets in a model of the North Atlantic, *J. Phys. Oceanogr.*, *39*, 1361–1379, doi:10.1175/2008JPO4096.1.

Kindle, J. C. (1986), Sampling strategies and model assimilation of altimetric data for ocean monitoring and prediction, *J. Geophys. Res.*, *91*, 2418–2432, doi:10.1029/JC091iC02p02418.

Ledwell, J. R., A. J. Watson, and C. S. Law (1993), Evidence for slow mixing across the pycnocline from an open-ocean tracer-release experiment, *Nature*, *364*, 701–703, doi:10.1038/364701a0.

Leith, C. E. (1973), The standard error of time-average estimates of climatic means, *J. Appl. Meteorol.*, *12*, 1066–1069, doi:10.1175/1520-0450(1973)012<1066:TSEOTA>2.0.CO;2.

Mariano, A. J., and O. B. Brown (1992), Efficient objective analysis of dynamically heterogeneous and nonstationary fields via the parameter matrix, *Deep Sea Res.*, *39*, 1255–1271, doi:10.1016/0198-0149(92)90068-5.

Maximenko, N., B. Bang, and H. Sasaki (2005), Observational evidence of alternating zonal jets in the world ocean, *Geophys. Res. Lett.*, *32*, L12607, doi:10.1029/2005GL022728.

Nakamura, M., and Y. Chao (2000), On the eddy isopycnal thickness diffusivity of the Gent-McWilliams subgrid mixing parametrization, *J. Clim.*, *13*, 502–510, doi:10.1175/1520-0442(2000)013<0502:OTEITD>2.0.CO;2.

Nakano, H., and H. Hasumi (2005), A series of zonal jets embedded in the broad zonal flows in the Pacific obtained in eddy-permitting ocean general circulation models, *J. Phys. Oceanogr.*, *35*, 474–488, doi:10.1175/JPO2698.1.

Pacanowski, R. C., and S. M. Griffies (1999), MOM 3 manual, technical report, Geophys. Fluid Dyn. Lab., Princeton, N. J.

Richards, K., N. Maximenko, F. Bryan, and H. Sasaki (2006), Zonal jets in the Pacific ocean, *Geophys. Res. Lett.*, *33*, L03605, doi:10.1029/2005GL024645.

Schiller, A., S. E. Wijffels, and G. A. Meyers (2004), Design requirements for an Argo float Array in the Indian Ocean inferred from Observing System Simulation Experiments, *J. Atmos. Oceanic Technol.*, *21*, 1598–1620, doi:10.1175/1520-0426(2004)021<1598:DRFAAF>2.0.CO;2.

Smith, R. D., M. E. Maltrud, F. O. Bryan, and M. W. Hecht (2000), Numerical simulation of the North Atlantic Ocean at 1/10 degrees, *J. Phys. Oceanogr.*, *30*, 1532–1561, doi:10.1175/1520-0485(2000)030<1532:NSOTNA>2.0.CO;2.

Treguier, A., N. Hogg, M. Maltrud, K. Speer, and V. Thierry (2003), The origin of deep zonal flows in the Brazil basin, *J. Phys. Oceanogr.*, *33*, 580–599, doi:10.1175/1520-0485(2003)033<0580:TOODZF>2.0.CO;2.

van Sebille, E., I. Kamenkovich, and J. Willis (2011), Quasi-zonal jets in 3D Argo data of the northeast Atlantic, *Geophys. Res. Lett.*, *38*, L02606, doi:10.1029/2010GL046267.

Vecchi, G. A., and M. Harrison (2007), An Indian Ocean Observing System Simulation Experiment, *J. Clim.*, *20*, 3300–3319, doi:10.1175/JCLI4147.1.

W. Cheng and D. E. Harrison, Joint Institute for the Study of the Atmosphere and Ocean, University of Washington, 3737 Brooklyn Ave. NE, Seattle, WA 98105-5672, USA.

I. Kamenkovich, Rosenstiel School of Marine and Atmospheric Science, University of Miami, 4600 Rickenbacker Cswy., Miami, FL 33149-1098, USA. (ikamenkovich@rsmas.miami.edu)

C. Schmid, NOAA Atlantic Oceanographic and Meteorological Laboratory, 4301 Rickenbacker Cswy., Miami, FL 33149, USA.